Volume 17
Number 17
7 May 2025
Pages 10393-11084

Nanoscale

rsc.li/nanoscale

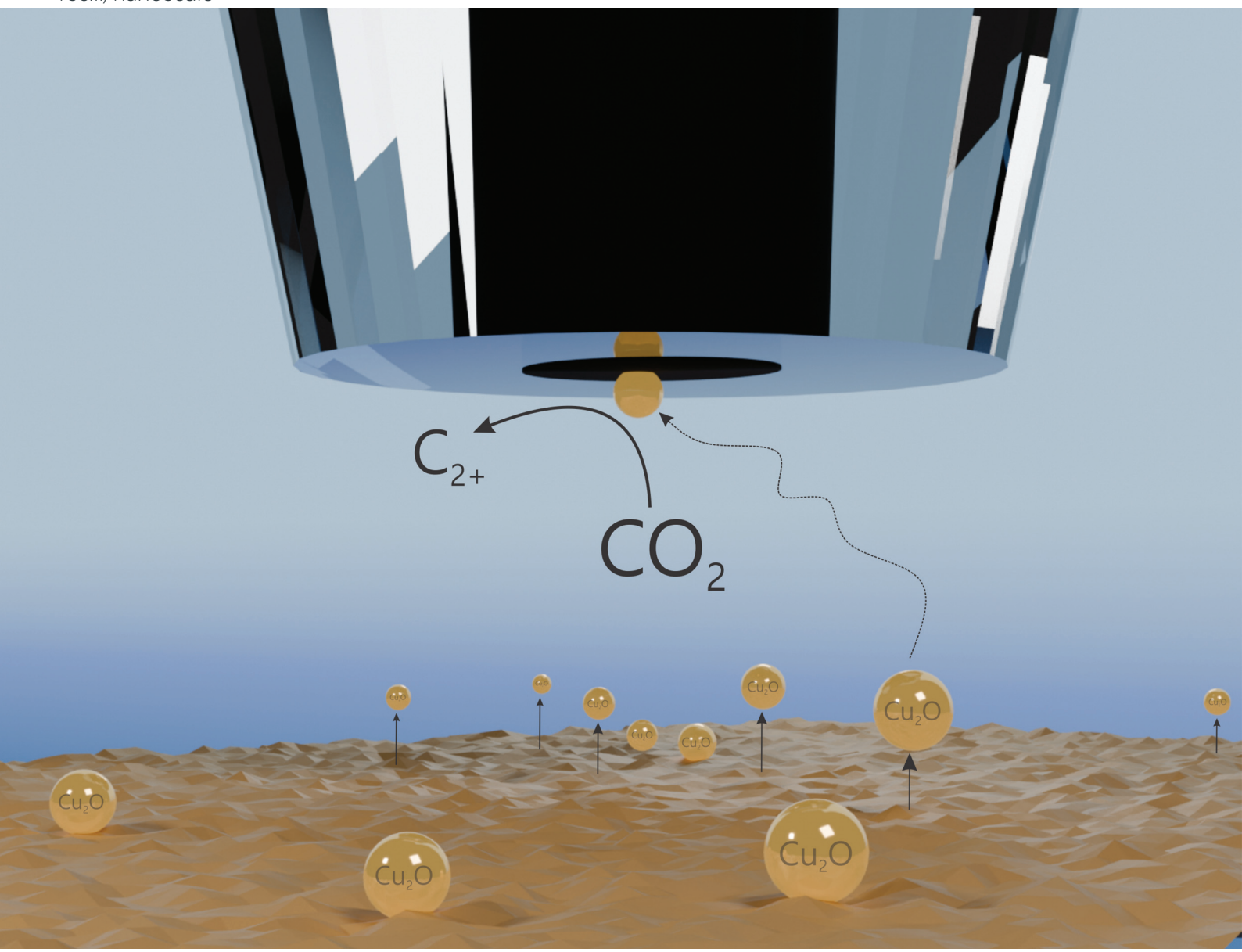

ISSN 2040-3372

ROYAL SOCIETY OF CHEMISTRY

PAPER
Talia Jane Stockmann *et al.*
Anodic expulsion of Cu nanoparticles from a polycrystalline Cu substrate: a novel corrosion and single entity study approach

NCNST

Nanoscale

ROYAL SOCIETY OF CHEMISTRY

PAPER

View Article Online
View Journal | View Issue

Cite this: *Nanoscale*, 2025, **17**, 10609

Anodic expulsion of Cu nanoparticles from a polycrystalline Cu substrate: a novel corrosion and single entity study approach†

Oforbuike N. Egbe, Bradley H. P. Morrissey, Francesca M. Kerton and Talia Jane Stockmann *

Cu is the dominant heterogeneous metal catalyst for CO_2 reduction (CO_2R) in combatting climate change, which often relies on Cu oxides (CuO or Cu_2O). This is complicated by the relatively facile reduction of Cu oxides to metallic Cu that precedes CO_2R, leading to potential morphological surface restructuring and lowered electrocatalysis. Herein, the anodic ejection of Cu/Cu oxide nanoparticles (NPs) from polycrystalline Cu is tracked through scanning electrochemical microscopy in substrate generation/tip collection (SECM-SG/TC) mode. Single entity electrochemical (SEE) detection of Cu^0 and Cu oxide NPs was recorded through the electrocatalytic amplification (ECA) of the CO_2R and O_2 evolution reaction (OER). The frequency (f) of NP impacts decreases concomitantly with increasing tip–substrate distance, while increasing the absolute value of the ultramicroelectrode (UME) tip potential (E_{tip}, negatively for CO_2R and positively for OER) resulted in an increase in stochastic NP impact peak current (i_p) commensurate with increasing overpotential. Complementary finite element simulations provide insight into the NP catalyzed CO_2R catalytic rate constants as well as the rate of passivation. If substrate oxidation is entirely avoided and cathodic E_{sub} maintained, then no NP ejection was observed. Anodic potentials are often used to oxidize Cu substrates making them more electrocatalytically active as well as to regenerate Cu oxide catalyst layers. We demonstrate that SEE detection offers a potential means of monitoring corrosion/loss of Cu material as well as quantitative kinetics measurement.

Received 19th November 2024,
Accepted 17th March 2025

DOI: 10.1039/d4nr04863f

rsc.li/nanoscale

1. Introduction

Cu remains the most effective metal candidate for CO_2 reduction (CO_2R) catalysis to value-added commodities.[1–4] Cu-alloys that favour maintaining Cu in the +1/+2 oxidation states are desirable since these have shown increased selectivity and enhanced faradaic efficiency towards methanol[2] or multi-carbon (C_{2+}) products.[5,6] Hu *et al.*[2] prepared Cu-based heterogeneous chalcogenide electrocatalysts such as Cu_3VS_4/CuVS to stabilize $Cu^{1+/2+}$ during the CO_2R to methanol and limit the hydrogen evolution reaction (HER). However, many approaches still rely on CuO/Cu_2O based materials due to their practicality since Cu has high affinity for oxygen.[7–9] Preparation typically includes the synthesis of CuO/Cu_2O nanoparticles (NPs) from polycrystalline Cu substrates *via* an electrode conditioning step,[7] wherein the metallic Cu electrode is first oxidized to form a Cu oxide surface layer. These can then be re-reduced to promote the formation of defects and grain boundaries which enhance electrocatalysis.[7]

Some reports indicated that Cu is dissolved and redeposited in a process termed cathodic corrosion which results in a morphological change of the Cu surface, *i.e.*, the development of different facets.[3,10–13] For example, Vavra *et al.*[10] explored the stability of CuO and Cu_2O NPs under CO_2R conditions and found that carbon monoxide (CO) and oxalate reduction products that adsorb on the metal surface also serve as ligands stabilizing dissolved Cu species, *e.g.*, through $[CuCO]^+$ formation. The Buonsanti group[10] as well as Speck and Cherevko[12] quantified the presence of dissolved Cu ionic species using in-line ICP-MS, with the former group employing ligands to stabilize Cu ions in solution. These analytical methods would likely be agnostic to whether the source of Cu was dissolved ionic species or Cu^0/Cu oxide NPs. A detailed voltammetric investigation of Cu surfaces with incidental anodic applied potentials as well as cathodic-only treatment gave strong evidence that in the latter case, Cu substrates showed no morphological change;[14] moreover, any change was likely owing to accidental oxidation or electrode fouling. Thus, the authors proposed that the reduction of unintended surface

Memorial University of Newfoundland, Chemistry Department, Core Science Facility, 45 Arctic Ave, St. John's, NL A1C 5S7, Canada. E-mail: tstockmann@mun.ca

†Electronic supplementary information (ESI) available: UME characterization details, the Cu Pourbaix diagram, altering E_{tip} investigations on CO_2R SEE, additional histogram data, IL coating experiments, and COMSOL Multiphysics finite element simulation details. See DOI: https://doi.org/10.1039/d4nr04863f

oxides during the CO_2R is what gives rise to the observed morphological changes.[14]

Indeed, recent real-time electrochemical liquid cell transmission electron microscopy (TEM)[8] revealed the degradation of Cu nanocubes and redeposition of nanoparticle (NP) fragments at CO_2R cathodic potentials (−1.1 V *vs.* the reversible hydrogen electrode, RHE). While intriguing, the development of gaseous products generating bubbles within the specialized cell prohibited long-term investigations.[8] Additionally, liquid cell TEM may not be able to observe the presence of suspended NPs owing to its limited depth-of-field/resolution power; for most TEMs, this is ~0.1 nm.[15] Nevertheless, Cu catalysts are possibly dynamic and may undergo morphological changes during sustained potentiostatic pulses necessary for electrolysis, particularly at anodic potentials. Depending on pH, Cu^0, CuO, and Cu_2O NPs can be ejected along with solubilized ionic species such as Cu^+, Cu^{2+}, and CuO_xH_y.[3] Examining the Pourbaix diagram for Cu at 25 °C,[16] the pH and potential in a region greater than 7 and ~0.0 V (*vs.* SHE), respectively, favour CuO(s)/Cu_2O(s) formation. While the local pH may increase during the CO_2R owing to the consumption of H^+ in the vicinity of the electrode, the use of $KHCO_3$ as a supporting electrolyte generally means operating at pH 7–10 in the bulk solution. Thus, during anodic Cu electrode conditioning or regeneration, CuO/Cu_2O NPs are likely formed and released into solution. Multiple groups have reported particulate matter formation in solution after prolonged potentiostatic pulses.[3,17] A recent study from Mena-Morcillo *et al.*[17] probing how redox mediators affect Cu substrates evidenced Cu accumulation on the inlaid disc, the Pt ultramicroelectrode (UME) after performing probe approach curves (PACs) during scanning electrochemical microscopy (SECM). However, they did not quantify the amount of the ejected Cu material.

Thus, based on the work discussed above, we hypothesized that not only are solvated Cu ions being released when Cu oxide modified electrodes are being regenerated (or during their initial modification), but also solid, Cu oxide nanoparticles (NPs). Since liquid-cell TEM lacks the depth-of-field to track NPs *in situ* and is still cost prohibitive, single entity electrochemistry (SEE) was employed herein to investigate the potential ejection of these Cu oxide NPs. Fig. 1 shows a diagram of the experimental setup and NP release mechanism.

SEE is an aspect of nanoelectrochemistry[18] and an evolving electroanalytical technique[19–23] with seminal contributions by Quinn *et al.*[24] as well as Xiao and Bard[25] towards polymer and metallic NP detection. Since then, Compton's group,[26] Kanoufi and co-workers,[22,27–29] Unwin's lab,[30–32] and many others[33–39] have greatly expanded the field of nanoelectrochemistry. 'Entity' can refer to a single molecule, NP, virus,[40] bacterium,[41] cell,[42] or atom.[41] These entities undergo Brownian motion within a solution and collide randomly with an ultramicroelectrode (UME) surface.[43] In the case of NPs, their interaction with the UME depends on their physicochemical properties; for example, a polymer NP may adsorb onto the UME surface lowering its overall surface area and blocking the current from a redox mediator.[24,44] Meanwhile, an electrocatalytic NP, such

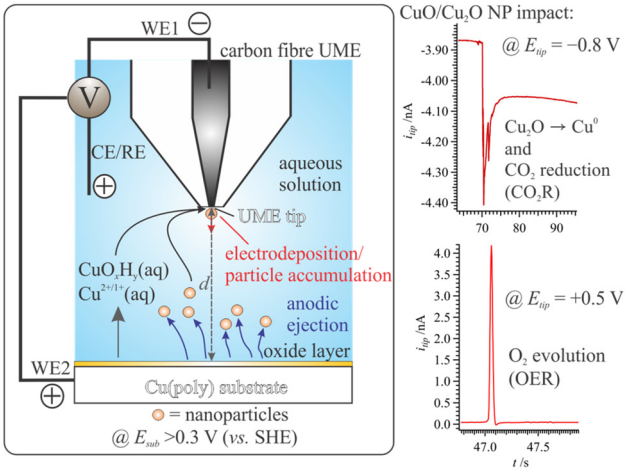

Fig. 1 Diagram of the scanning electrochemical microscope in the substrate-generation/tip-collection (SECM-SG/TC) configuration using a bipotentiostat, wherein working electrodes (WEs) 1 and 2 were connected to the carbon fibre ultramicroelectrode (UME) and polycrystalline Cu substrate (Cu(poly)), respectively. A Pt counter and Ag/AgCl reference electrodes were employed; however, these have been merged in the image above for simplicity. The right-hand side depicts the typical nanoparticle (NP) impact profiles when the tip potential (E_{tip}) is biased at −0.8 and +0.5 V (*vs.* SHE), while the substrate (E_{sub}) is biased at +0.3 V in a pH 10 solution.

as Pt NPs, may enhance the electrocatalytic current associated with various interfacial charge transfer reactions, *e.g.*, the H_2 evolution or O_2 reduction reaction.[22,25] This process is commonly referred to as electrocatalytic amplification (ECA).[18,23,26,45–47] Alternatively, metal NPs can be oxidatively deconstructed into their constituent ions. For example, Ag NPs are often employed to investigate oxidative dissolution since Ag is typically fully ionized during oxidation and dissolved, *i.e.*, $Ag^0(s) \rightarrow Ag^+(aq) + e^-$.[48,49]

Herein, PACs were performed to position a carbon fibre UME close to a polycrystalline Cu substrate (Cu(poly)) electrode surface and monitor the loss of both solvated Cu ionic species and NP materials through stochastic impacts of any Cu^0, CuO, or Cu_2O NPs through SEE detection *via* the ECA[23,45] of either CO_2R or O_2 evolution (OER) as well as CuO/Cu_2O NP reduction (see Fig. 1). The accumulation of the Cu electrodeposited material as well as the presence of Cu oxide NPs was confirmed using scanning (SEM) and transmission electron microscopy (TEM) of the UME tip and aqueous electrolyte phase. Interestingly, Cu^0/Cu oxide NP ejection was only observed if the polycrystalline substrate was exposed to anodic potentials. This agrees with the work of Raaijman *et al.*[14] as well as Speck and Cherevko.[12]

2. Experimental methods

2.1. Chemicals

All chemicals were used as received without purification unless otherwise indicated. Copper foil (0.1 × 100 × 1000 mm,

99%) was purchased from USA–Mily (China), while ferrocene methanol ($FcCH_2OH$, 97%), trihexyltetradecylphosphonium bis(trifluoromethylsulfonyl)imide ($P_{66614}NTf_2$, >95%), isopropanol (>99%), and potassium bicarbonate ($KHCO_3$, 99.7%) were sourced from Sigma-Aldrich. Potassium hydroxide (KOH, 88.7%) was bought from Fisher Scientific and potassium chloride (KCl, 96%) from Anachem Ltd. All aqueous solutions were prepared with ultrapure water (18.2 MΩ cm) obtained from a Millipore filtration system. Alumina oxide polishing slurry (Buehler) of 0.5–3 μm was used to polish the polycrystalline Cu substrate before use.

To modify or coat the Cu substrate with ionic liquid (IL), approximately 21.5 mg of $P_{66614}NTf_2$ was dissolved in 1 mL isopropanol solvent. The solution was sonicated for 5 min, and then 100 μL of solution was drop-cast on a mirror-polished polycrystalline copper (Cu(poly)) plate. The exposed Cu surface area for the SECM-SG/TC (scanning electrochemical microscopy in substrate generation/tip collection mode) study was ~1 cm^2 as calculated from the radius (0.564 cm) of the circular cell aperture.

2.2. Instrumentation

All electrochemical measurements were performed using the ElProScan potentiostat (Heka Elektronik) with a 3-axis positioner in 3- or 4-electrode mode in which Pt and Ag/AgCl served as counter and reference electrodes, respectively. A carbon fibre UME and the Cu(poly) substrate served as working electrodes 1 and 2 (see Fig. 1) in SECM SG/TC mode. Further details about UME characterization can be found in the ESI section 1.† All potentials were referenced to SHE unless otherwise indicated.

Scanning (SEM) and transmission electron microscopy (TEM) experiments were performed using the JEOL JSM 7100 F with energy dispersive X-ray (EDX) and Tecnai Spirit Transmission Electron Microscope, respectively. EDX data were analyzed using DTSA II software released by the National Institute of Standards and Technology (NIST) in the US, see **https://www.nist.gov/services-resources/software/nist-dtsaii**.

A pH meter (sympHony model# B10P, VWR) was used to measure the acidity of aqueous solutions.

2.3. Peak analysis

The stochastic Cu oxide NP peak analysis, including integration for calculation of the charge transferred (Q) and peak current (i_p) as well as impact duration, was performed using a specialized code written in Python software. This code is freely available on GitHub (**https://github.com/Bmor9421/Ionosome-Data-Analysis-Code**) as previously reported by our group.[19]

3. Results and discussion

Fig. 2 shows the cyclic voltammograms (CVs) initially recorded at the Cu(poly) substrate with a circular 1 cm^2 exposed surface area (r = 0.564 cm) at a scan rate of 0.020 V s^{-1} in $KHCO_3$ at pH 10. All experimental potentials have been referenced to SHE unless otherwise noted. The black, solid trace was initiated at the open-circuit potential (OCP) of roughly −0.1 V (*vs.* SHE) and then swept cathodically. A peak-shaped cathodic wave was observed at −0.22 V, which is likely CuO reduction to Cu_2O.[9,13,50–52] The proposed surface reactions have been written inset in Fig. 2. The Cu(poly) substrate was stored in a desiccator and polished using and alumina oxide slurry before use but otherwise not given special treatment; thus, it was exposed to air during shipping and handling inducing some surface oxidation. Continuing negatively, a second cathodic signal was recorded at −0.68 V which is the further reduction of any Cu surface oxides Cu_2O to metallic Cu. Meanwhile, a complex anodic signal was observed at roughly −0.05 V during the positive scan which is likely the adsorption of OH^- and subsequent oxidation of the Cu^0 surface, *i.e.*, Cu → Cu-$OH_{(ads.)}$ → Cu_2O → CuO.[9,13,50–52]

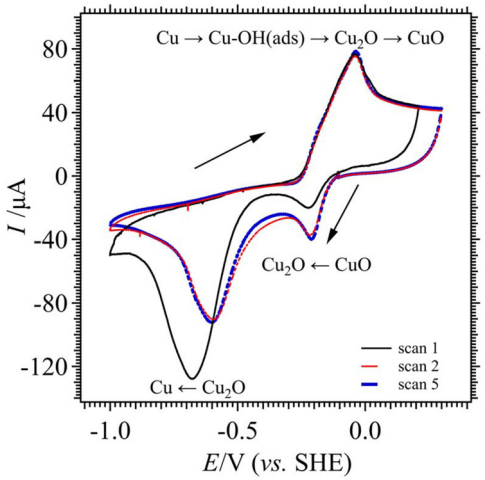

Fig. 2 Cyclic voltammograms (CVs) recorded using a polycrystalline Cu (Cu(poly)) substrate with a surface area of 1 cm^2, in a $KHCO_3$ solution adjusted to pH 10 (~0.5 M $KHCO_3$), at a scan rate of 0.020 V s^{-1}. The proposed surface reactions for each anodic and cathodic peak signal have been added in the inset. Multiple consecutive scans were performed as indicated in the inset.

These data in Fig. 2 and peak assignments agree well with Kim *et al.*,[9] who showed the restructuring of Cu(poly) → Cu(111) → Cu(100) in 0.1 M KOH through *operando* electrochemical scanning tunnelling microscopy (EC-STM), wherein, voltammetrically, the presence of a 2Cu → Cu_2O anodic peak at roughly 0.05 V *vs.* SHE and a re-reduction signal of Cu_2O to 2Cu at −0.38 V *vs.* SHE was shown. Both responses are in good agreement with the data shown in Fig. 2. The OCP at −0.1 V lies in between the observed CuO → Cu_2O cathodic and Cu → CuO anodic waves.

Moreover, Bodappa *et al.*[51] evidenced the formation of surface Cu oxide species using shell-isolated nanoparticle-enhanced Raman spectroscopy (SHINERS), wherein Au coated SiO_2 nanoparticles were dispersed across a Cu(111) or Cu (poly) surface. The authors proposed the following surface transformations at Cu(111) with increasing anodic potential

versus the reversible hydrogen electrode (RHE) in a pH 12 KOH solution,[51]

$$Cu + H_2O \rightarrow Cu\text{-}OH_{(surf)} + H + e^- E < 0\ V\ vs.\ RHE \quad (1)$$

$$Cu\text{-}OH_{(surf)} \rightarrow Cu\text{-}O_{(surf)} + H^+ + e^- E = 0\text{–}0.5\ V\ vs.\ RHE \quad (2)$$

$$Cu\text{-}O_{(surf)} \rightarrow Cu_2O_{(surf)} + e^- E = 0.55\ V\ vs.\ RHE \quad (3)$$

These potential values translate to −0.71 to −0.16 V *vs.* SHE at pH 10, which is in fair agreement with the Cu(poly) values described above. Bodappa *et al.*[51] only observed OH adsorption at Cu(poly), but not further Cu oxidation; however, since they performed their experiments at pH 12, CuO and Cu_2O formation is not expected as demonstrated through thermodynamic calculations for the Pourbaix diagram at 25 °C.[16]

During the second CV in Fig. 2, the cathodic peak at −0.68 V shifts towards positive potentials (−0.59 V), while the magnitude of the CuO → Cu_2O cathodic current signal increases. The former is likely owing to a shift in the local pH owing to the CO_2R which consumes H^+ in the vicinity of the Cu(poly) surface lowering the overall required driving force for reduction. The latter is the result of the accumulation of surface oxides generated by sweeping the potential. Subsequent scans showed good overlap indicating a steady state condition, as can be seen in scan 5, the thick, blue, and dashed trace in Fig. 2.

A sample of the solution was deposited on a TEM grid after pulsing the substrate at E_{sub} = 0.3 V for ~10 min and imaged (see Fig. S2 of the ESI†) which showed the presence of nanoparticles with a bimodal distribution. Larger NPs were mostly spherical; however, some were cubic with an average size of 450 ± 80 nm (see Fig. S2 of the ESI†). Smaller, spherical particles were also imaged with a size distribution of 5.6 ± 1.0 nm. EDX analysis (data not shown) indicated that the NPs are composed of Cu and O in roughly equal proportions, *i.e.*, likely CuO NPs. Thus, under sufficient anodic polarization, the Cu(poly) substrate will eject CuO NPs.

Next, using 0.9 mM ferrocene methanol ($FcCH_2OH$) as a redox mediator in 10 mM KCl aqueous electrolyte solution, the UME tip (r_a = 3.5 μm) was positioned at a tip-to-substrate distance (d) 2 μm away from the Cu substrate *via* a probe-approach curve (PAC, see ESI section 1† for details) experiment. Subsequently, the $FcCH_2OH$ solution was removed and replaced with a KOH or $KHCO_3$ solution adjusted to pH 13 (~0.1 M KOH) or 10 (~0.5 M $KHCO_3$), respectively. No other supporting electrolyte was added.

The blue, dashed trace in Fig. 3A depicts the CVs recorded at the UME tip with d = 2 μm while the Cu(poly) substrate was biased (E_{sub}) at ~0.3 V (*vs.* SHE). E_{sub} = 0.3 V was chosen as it was well above the measured Cu oxidation potentials observed in Fig. 2 to ensure maximum generation of the Cu oxide material. Initially, the UME recorded a negative current signal with an onset potential at roughly −0.8 V during the cathodic sweep (blue, dashed trace in Fig. 3A) using $KHCO_3$ (pH 10). This corresponds to HCO_3^-/CO_2 reduction (CO_2R) as well as H_2 evolution (HER). No O_2 reduction wave was observed. Since

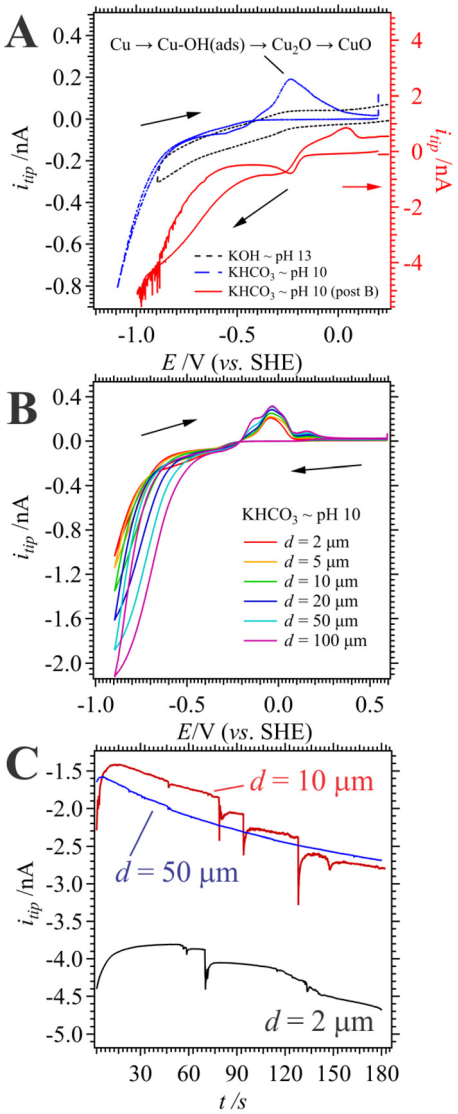

Fig. 3 (A) Cyclic voltammograms (CVs) recorded in KOH (pH 13) or $KHCO_3$ (pH 10), *i.e.*, ~0.1 M KOH or ~0.5 M $KHCO_3$, respectively, solutions at the tip of a 7 μm diameter carbon fibre UME, with d = 2 μm above the Cu(poly) substrate, v = 0.020 V s^{-1}, and E_{sub} = 0.3 V *vs.* SHE. The blue dashed and red solid traces were recorded using the UME at pH 10 in $KHCO_3$ at d = 2 μm before and after, respectively, the SECM distance experiments shown in (B). The red, dashed arrow indicates the axis the trace has been plotted against. (B) UME (i_{tip}) i–E curves recorded with increasing d values as indicated in the inset, with E_{sub} = 0.3 V. (C) Chronoamperograms recorded with increasing d values as indicated in the inset with E_{sub} = 0.3 V and E_{tip} = −0.60 V (*vs.* SHE). Voltammetric scan rates (v) of 0.020 V s^{-1} were used throughout.

E_{sub} was held at 0.3 V, during the electrooxidation the generation of soluble, ionized Cu species may take place whose standard reduction reactions are given below,[53]

$$Cu^{2+}(aq) + 2e^- \rightarrow Cu(s)\ E° = 0.3419\ V \quad (4)$$

$$Cu^{+}(aq) + e^- \rightarrow Cu(s)\ E° = 0.521\ V \quad (5)$$

$$Cu(OH)_2(aq) + 2e^- \rightarrow Cu(s) + 2OH^-(aq)\ E^\circ = -0.222\ V \quad (6)$$

Thus, the CO_2R/HER signal could be convoluted by the re-reduction of Cu ionized species, *i.e.*, Cu^0 electrodeposition (eqn (4)–(6)). Indeed, during the tip anodic scan (Fig. 3A, blue dashed trace), a peak-shaped wave was observed at −0.25 V which is likely associated with oxidation of Cu^0 now on the UME surface, *i.e.* eqn (1)–(3). Thus, while no independent $CuO/Cu_2O \rightarrow Cu^0$ cathodic wave was observed, ionized Cu species are likely being deposited. Interestingly, a so-called 'nucleation loop' was observed,[54] wherein the voltammetric scan crosses over itself during the reverse potential scan at roughly −0.7 V. A nucleation loop is consistent with a change in the interfacial surface area as species are electrodeposited onto an electrified surface as shown by electropolymerization of conductive polymers by Heinze *et al.*[54] on an electrode surface as well as more recently at the immiscible, electrified liquid|liquid interface.[55–57] These results of Cu electrodeposition and dissolution agree with previous thermodynamic calculations (see also Fig. S3 of the ESI†).[16] When the $KHCO_3$ solution was swapped for 0.1 M KOH at pH 13, the coupled Cu_2O/Cu^0 and CO_2R signals greatly reduced in magnitude (dashed, black trace in Fig. 3A). This likely results from the lower HCO_3^-/CO_2 concentration which decreases the effective CO_2R. In either case, in this pH regime and at the HCO_3^- concentrations employed, the O_2 reduction signal is likely a minor contributor, while simultaneously the HER is suppressed at alkaline pH.[58]

Subsequently, *i*–*E* curves were recorded in 0.1 M $KHCO_3$ (pH 10) at E_{sub} = 0.3 V with the UME positioned at d = 2 μm and then d was incrementally increased up to 100 μm as shown in Fig. 3B. The concomitant increase in CO_2R signal/Cu^0 deposition current is attributed to the increasing amount of Cu species released into solution from the substrate as the experiment progressed. Increasing Cu dissolved ionic species results in an increasing amount of Cu^0 electrodeposited on the UME surface, which in turn increases its electroactive surface area (ESA). As mentioned above, Cu has been shown to be a good CO_2R electrocatalyst,[2,7,8] while the carbon fibre is not; thus, the increasing current signal is also likely owing to increasing Cu mediated CO_2R electrocatalysis owing to the presence of an increased amount of Cu on the UME surface, which in turn expands its ESA. In other words, the UME is more electrocatalytically active and has a higher surface area. Indeed, when the tip was returned to d = 2 μm and a CV was recorded (red, solid curve in Fig. 3A), a cathodic peak-shaped wave at −0.23 V was observed which is likely a combination of CO_2 and $CuO \rightarrow Cu_2O$ reduction. Additionally, large, negative current spikes began appearing at roughly −0.7 V. It was hypothesized that these may be owing to stochastic Cu^0/Cu oxide NP impact events. Indeed, Beverskog and Puigdomenech[16] indicated that CuO(s) and Cu_2O(s) species are thermodynamically stable in this pH/E_{sub} regime. Thus, these data would be consistent with CuO/Cu_2O NP impacts detected through the ECA[19,20,22,26,45,46,59] of the CO_2R.

To explore this, chronoamperograms (CAs) were recorded with E_{sub} = 0.3 V and E_{tip} = −0.6 V using $KHCO_3$ (pH 10) at increasing d (see Fig. 3C). At d = 2 μm current spikes reminiscent of SEE impacts were observed with the onset of the characteristic sharp, negative peak current (i_p) followed by an exponential decay that often does not return to the baseline, *i.e.*, a current step (see also Fig. 1 for magnified *i*–*t* pulses). As d increased, the impact frequency (f) and i_p intensity decreased concomitantly (see Fig. 4A). This is consistent with larger NPs having smaller diffusion coefficients, and thus, taking longer to arrive at the UME tip surface. The NP diffusion coefficient (D_{NP}) can be calculated using the Stokes–Einstein relationship (eqn (7)),[23,46,47] wherein k_B, T, η, and r_{NP} are the Boltzmann constant (1.381×10^{-23} J K^{-1}), absolute temperature (295.15 K), viscosity of water (0.954 mPa s), and particle radius, respectively.

$$D_{NP} = \frac{k_B T}{6\pi\eta r_{NP}} \quad (7)$$

One can further access D_{NP} through its relationship with f *via* eqn (8),[23,46,47]

$$f = 4c_{NP}D_{NP}r_a \quad (8)$$

in which r_a is the radius of the electroactive disc of the UME and c_{NP} is the NP concentration. Since these NPs are dynamic and generated *in situ*, D_{NP} or c_{NP} are difficult to measure

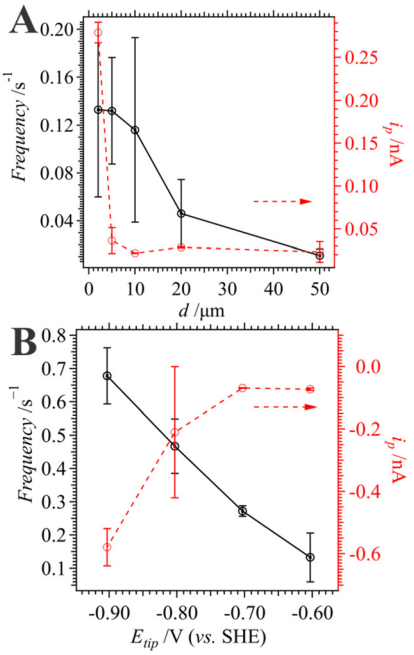

Fig. 4 (A) Plot of the stochastic NP impact frequency and peak current (i_p) *versus* d as determined from the analysis of *i*–*t* curves (see Fig. 1C). Red, dashed arrow indicates the axis, while error bars are one standard deviation (σ) or 3σ in the case of frequency (f) and i_p, respectively. (B) Plot of the change i_p (red, dashed curve) and f (black, solid trace) *versus* E_{tip} (see ESI Fig. S6 and S8†). Red, dashed arrow indicates the curve in the *y*-axis.

directly. Nevertheless, f is likely proportional to the rate of corrosion. The use of eqn (8) assumes the ESA of the UME is not changing; however, the results above strongly indicate that Cu electrodeposition on the UME surface is taking place. Thus, the use of eqn (8) is approximative and used here for simplicity. Future work will include the development of a computational model to try and account for the changing ESA of the UME.

Fig. 5A–E depict SEM micrographs of the Cu substrate and UME tip obtained before and after the oxidative series of experiments described in Fig. 3 as well as after oxidation in ~0.1 M KOH (pH 13). The unreacted substrate is smooth and featureless; however, oxidation at pH 10 generates cubic NPs dispersed across the surface. At pH 13, the smooth Cu(poly) surface is converted to needle-like structures. Similarly, the UME surface is bare before but covered in a deposit of Cu^0 or Cu oxide NPs afterwards (Fig. 5B and D). To quantify the level of Cu electrodeposition, a series of tests were performed in $KHCO_3$ (pH 10) with a freshly polished UME positioned at d = 10 μm above the Cu(poly) substrate which was biased at E_{sub} = 0.3 V, while E_{tip} was biased at −0.8 V for 3–12 min (see section 3.0 of the ESI†). The UME was polished after SEM imaging, between each test. The height of the Cu deposit was measured using ImageJ software and found to increase concomitantly with increasing pulse duration, wherein after 3 min it was roughly 1.12 μm, while after 6, 9, and 12 min it increased to 1.19, 2.47, and 2.54 μm, respectively. However, the shape is not uniform, as can been seen in Fig. S4C† after 12 min of electrodeposition, the deposit tends towards a cauliflower-like appearance spreading outwards in multiple directions. The Cu growth would impact the effective tip-to-substrate distance. Direct contact with the substrate would result in a closed circuit between WE1 and WE2 that would generate a massive current increase owing to the good conductivity of the Cu electrodeposited layer and the substrate; however, this was not observed indicating fairly good tip–substrate separation. If E_{sub} is maintained at the OCP, then no electrodeposit was observed at either negative or positive tip potentials (data not shown). The observation of Cu deposits on the UME surface agrees well with observations made by Gateman's group during their investigation of the redox mediator effect on Cu corrosion.[17] Thus, the UME interface itself is dynamic with an evolving ESA owing to Cu^0 and Cu oxide electrodeposition and possible morphological restructuring.

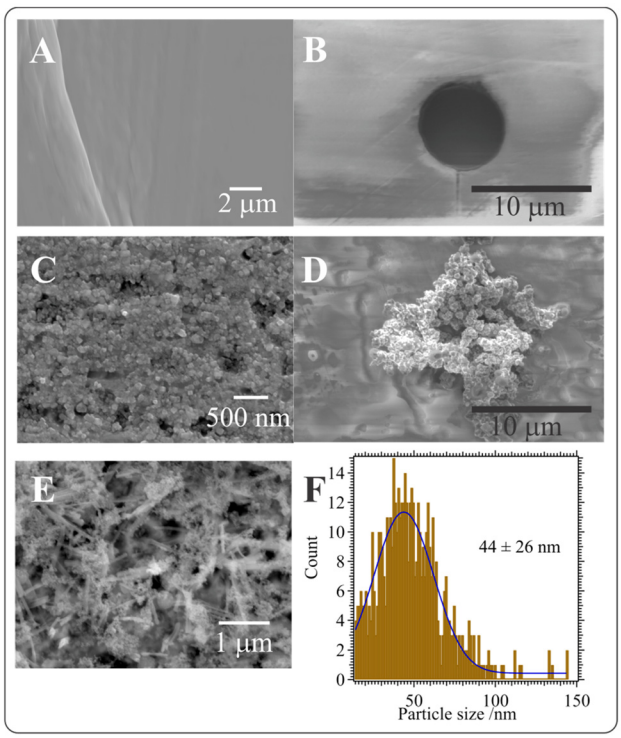

Fig. 5 Scanning electron microscopy (SEM) micrographs of the initial polycrystalline Cu substrate (A) and after oxidation in pH 10 $KHCO_3$ (C) or pH 13 KOH (E). SEM images of the UME tip before (B) and after (D) the SECM tip distance experiments detailed in Fig. 1. (F) Histogram of NP sizes sampled from C using ImageJ software. The blue curve is a Gaussian curve fitting generated using Igor Pro software (version 9.0.5).

Subsequently, i–t curves were obtained with a tip-to-substrate distance of d = 2 μm while maintaining E_{sub} = 0.3 V and biasing the UME tip potential, E_{tip}, at −0.6 to −0.8 V (see Fig. S5 of the ESI†). Fig. 4B plots the change in i_p and f with changing E_{tip}. There is a steady increase in f and i_p as the magnitude of E_{tip} is increased. Since an increase in the applied potential in turn increases the CO_2R overpotential, this would improve CuO/Cu_2O mediated electrocatalysis. Thus, during NP impact, this would increase the average i_p. The larger i_p means that smaller NPs can be detected *via* ECA, contributing to a higher observed f.

Lacking tandem *in situ* optical techniques (*e.g.*, darkfield optical microscopy), the Cu oxide NPs in Fig. 5C were used to provide an approximate size. Cubes were measured along their longest edge using ImageJ software. Fig. 5F shows the histogram developed. Using a Gaussian distribution fitting, an average size of r_{NP} = 44 ± 26 nm was obtained. If one assumes that (i) $r_{NP} \approx 44$ nm; (ii) the NP volume is $V_{NP} = (r_{NP})^3$; (iii) these are all CuO NPs (M_w = 79.55 g mol^{-1}, ρ = 6.315 g cm^{-3}); and (iv) the UME surface area does not change, then *via* eqn (8) the loss of the CuO particulate material can be calculated. Admittedly, based on the discussion above concerning the changing ESA of the UME, this 4th assumption is highly approximative. Additionally, eqn (7) is applicable to spherical particles and is used here for simplicity.[60,61] While suspensions of cubic particles can often give rise to non-Newtonian fluid dynamics at high shear stresses, this is likely not the case here.[60,61] Thus, one may consider this a fifth assumption.

Fig. S9† shows the graph generated of c_{NP} determined using the f data and eqn (8) *versus* either d or E_{tip}, wherein, while E_{tip} was varied, d was held at 2 μm, and when d was changed, E_{tip} was maintained at −0.6 V. With increasing d, larger NPs are not able to travel to the UME tip surface within the timeframe of the chronoamperometric experiment, as described above; thus, f and c_{NP} drops significantly (see also Fig. 4A). With changing d, Fig. S9† provides a rough anodic expulsion profile highlighting the distance Cu oxide particles travel above the

Cu(poly) substrate, with many smaller particles reaching a height of 50–100 μm. If one assumes that the growing Cu deposit conforms to the shape of a truncated spheroid (*i.e.*, sphere-cap), then Alfred and Oldham's equations[62] for such UMEs can be used in place of eqn (8), and the c_{NP} profile can be further refined. However, this is beyond the scope of the present work.

Nevertheless, this insight can be especially useful in designing electrolysis cells/reactors and positioning counter (CE) or reference (RE) electrodes. Indeed, if the reoxidation of CO_2R products at the CE can be mitigated or overcome, one can imagine constructing an electrocatalytic cell in which this NP anodic expulsion is exploited to capture stray nanocatalysts. Moreover, these results highlight nanocatalyst loss which is particularly important to electrocatalysis in flow cell configurations especially during electrocatalyst regeneration cycles that involve anodic potentials. A UME positioned downstream might be able to track this loss through SEE and provide an indication of when a nanofunctionalized electrode needs to be swapped out.

Cu oxide NPs have also been employed as heterogeneous OER catalysts.[63] Fig. 6A and B show CVs recorded at pH 13 and 10, in KOH solutions, respectively. The former favours solubilized $Cu_x(OH)_y^{z+}$(aq) species while the latter the formation of Cu oxide NPs at potentials >0.1 V (see Fig. S3†).[16] The blue trace in Fig. 6A shows i_{tip} in which the anodic peak at 0.47 V is likely the Cu to CuO oxidation pathway, and the cathodic peaks at 0.26 and −0.5 V are the respective $CuO \rightarrow Cu_2O$ and $Cu_2O \rightarrow Cu^0$ reduction signals. Chronoamperograms performed at pH 13 with E_{sub} = 0.3 V and E_{tip} = −0.8 or 0.5 V showed no NP impact events, see Fig. 6C and E, respectively. Even when pulsing E_{sub} to much more positive potentials (Fig. 6E) no impact transients were recorded. These results are consistent with the Pourbaix diagram in which solubilized Cu ionic species are formed, *i.e.*, no Cu oxide NPs are generated. However, Cu ionic species reduction and electrodeposition continues as evidenced by the negative slope of the *i*–*t* responses shown in Fig. 6C. If the KOH solution pH is adjusted down to pH 10, then large current spikes were observed while E_{tip} was maintained at 0.5 or 0.7 V, see Fig. 6D and F, respectively. However, these NP impact responses are owing to the ECA of the OER rather than the CO_2R. The benefit of targeting the OER is that one avoids simultaneous Cu ionic species electrodeposition; thus, this is a less dynamic potential region.

To investigate potential Cu oxide NP accumulation on the UME surface, similar to the CO_2R case above, the UME was positioned at d = 10 μm above the Cu(poly) substrate with E_{tip} and E_{sub} maintained at 0.5 and 0.3 V, respectively, for 9 min. Fig. S6A–S6C† shows the SEM images of the UME tip after the *i*–*t* pulse was applied. At pH 10, in either $KHCO_3$ or KOH solutions, the accumulation of Cu NPs were observed; however, when the pH was increased to 13, NPs were not present (Fig. S6B†). EDX analysis (data not shown) indicates that for the pH 10 $KHCO_3$ case, the NPs are mostly composed of Cu with trace amounts of O. Meanwhile, the pH 10 KOH solution showed a ratio of 1.2 : 1 of Cu : O likely indicating that the NPs are mostly CuO. In the pH 10 KOH case (Fig. S6C†), the NPs are distributed around the outside edge of the carbon fibre disc and projecting inwards, while for $KHCO_3$ pH 10, the NPs are spread across the surface as well as in two clumps along the glass sheath on either side of the carbon fibre disc. The presence and adsorption of Cu and Cu oxide NPs on the UME surface at this applied tip potential is somewhat surprising and may be due to an electrostatic interaction between the NPs and the carbon fibre.

Often before performing electrolysis in CO_2R programs, the aqueous solution is bubbled with CO_2(g) to increase [CO_2](aq) and purge other gases, *e.g.,* O_2; however, this lowers the pH from 10 to 7–8 through the formation of carbonic acid. At pH 7–8 one is on the cusp of two Cu stability regimes (see Fig. S3†),[16] wherein at potentials greater than ∼0.2 V, Cu^{2+}(aq) is stable at pH < 7, while CuO(s) is stable at 7 < pH < 13. Thus, up to this point, solutions were not bubbled with CO_2 to avoid any ambiguity. Fig. S10A and S10B of the ESI,† however, depicts the CV and chronoamperometric UME tip responses, respectively, with it positioned at d = 10 μm with E_{sub} = 0.3 V if the solution is bubbled for ∼30 min with CO_2(g). The voltammetric cathodic peak signal at $E_{tip} \approx -0.7$ V increases once the solution is purged with CO_2 (red trace in Fig. S10A of the ESI†). If the Cu(poly) substrate is not present and biased at E_{sub} = 0.3 V, opposite to the UME tip, then no cathodic signal was observed at this potential (Fig. S10C in the ESI†). Thus, the cathodic wave observed in Fig. S10A† is a combination of CO_2R and Cu electrodeposition. The chronoamperometric pulse in Fig. S10B of the ESI† after purging with CO_2(g) does have peak current transients; however, the frequency is too high to resolve individual impact events likely owing to the exceptionally high [CO_2](aq). Thus, no useful data can be interpreted.

Similar to the CO_2R investigation described above, as E_{tip} increases anodically, there is a concomitant increase in i_p and f for the impact events during the OER (see Fig. S12 of the ESI†). SECM imaging using $FcCH_2OH$ redox mediator of the pristine and oxidized Cu(poly) substrate, see Fig. S13A and S13B of the ESI,† respectively, indicate that the latter is more electroactive in some areas, but there is a definite loss of electroactivity in others. These data are consistent with SECM metal corrosion responses.[17,31,64]

To investigate if the Cu substrate could be modified to inhibit NP expulsion, it was first coated with a thin layer of hydrophobic ionic liquid (IL), $P_{66614}NTf_2$, see Fig. S14.† During the PAC experiment to position the UME tip at d = 2 μm above the Cu(poly)/IL substrate, a pure insulating, negative feedback response was recorded (data not shown), and initial *i*–*t* recordings demonstrated virtually no impact responses (Fig. S14A†) even after multiple pulses. However, optical images taken at 4× magnification with a CCD camera showed that the IL film was not homogeneously distributed across the surface (see Fig. S14C†). Repositioning the UME above an area which appeared to have a thinner IL coating elicited apparent stochastic impacts (Fig. S14B†); however, the maximum i_p was

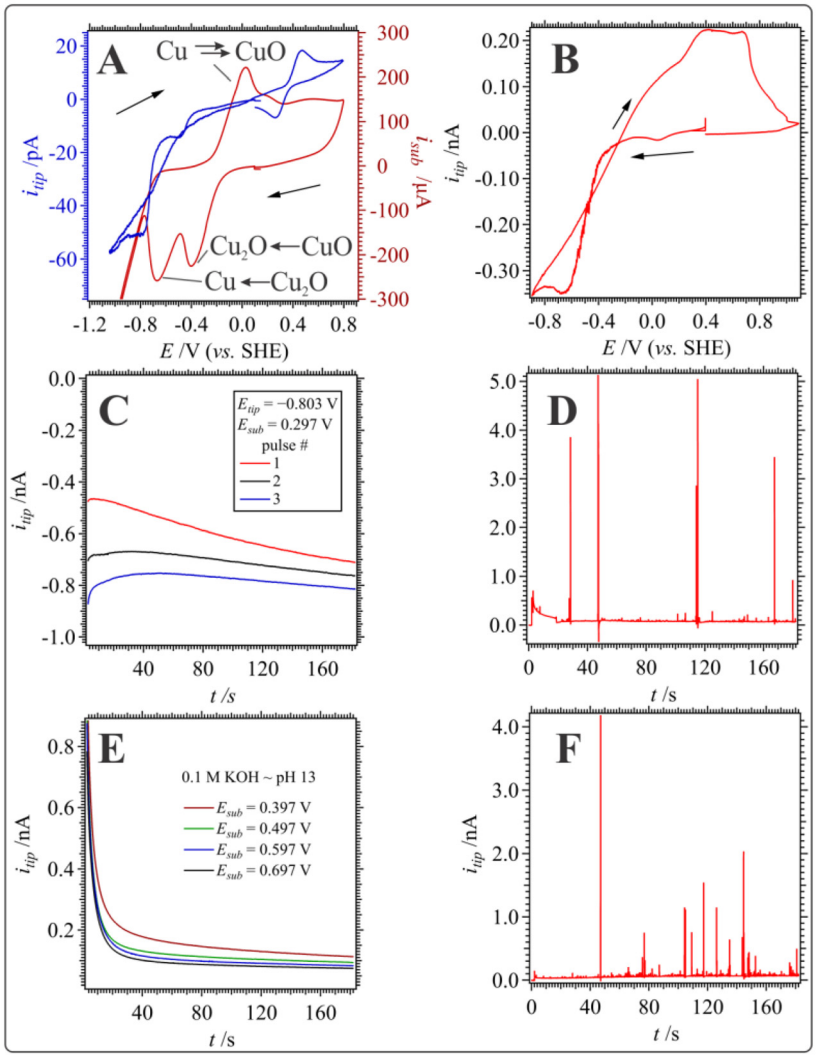

Fig. 6 CVs measured at 0.020 V s^{-1} in a roughly pH 13 (A) and 10 (B) KOH solution. Chronoamperograms obtained at d = 2 μm at pH 13 KOH using the same UME as in Fig. 1 after polishing; however, using E_{tip} = −0.80 (C) and 0.3 V (E) with E_{sub} = 0.3 V and as shown in the inset (*vs.* SHE), respectively. Additional *i*–*t* curves recorded at pH 10 using KOH with E_{sub} = 0.3 V, while E_{tip} was set to 0.5 (D) and 0.7 V (F). Measurements were performed using a carbon fibre UME (r_a = 3.5 μm) positioned at d = 2 μm.

greatly reduced compared to the bare Cu(poly) substrate which was maintained over several *i*–*t* pulses. Fig. S14D–F† show the histograms created through current spike analysis of the first 3 *i*–*t* traces shown in Fig. S14B.† The mean spike duration was similar to those shown in Fig. 3C for the Cu(poly) substrate alone which may indicate similar passivation kinetics. Moreover, coating the nanofunctionalized catalyst layer with materials such as ILs, or potentially Nafion, can be a strategy towards mitigating nanocatalyst loss. SEE can be employed as a direct measure of their effectiveness.

The mean duration for the ECA of CO_2R impact events was ~0.2 s which is greater than 2× the length of OER ones at ~0.06–0.07 s. Since NPs in the CO_2R case tend to stick/electrodeposit onto the UME surface more than at OER potentials, and as mentioned above, the CO_2R signal is convoluted by the reduction of Cu oxides to Cu^0, *e.g.*, $Cu_2O \rightarrow 2Cu$, the decay in the peak current transients must be the result of NP passivation. Since Cu is more electrocatalytically active in the Cu^{2+} or Cu^{1+} state than Cu^0,[2] this could be the source of the decay current and be seen as effective passivation. To study the possible kinetics of this passivation effect, a finite element model in COMSOL Multiphysics was constructed (see ESI section 7†). This model is similar to the one described recently by Klinkova's group[65,66] in which the electric double layer (EDL) is simulated using a Stern model to effectively simulate the interfacial potential drop, while also using Bulter–Volmer kinetics to describe the CO_2R. To approximate the passivation kinetics, the standard rate constant (k°) within the Butler–Volmer equation (see eqn (S3)–(S5) of the ESI†) was replaced with the following relationship,

$$k^\circ(t) = k_i(1 - e^{-at}) \quad (9)$$

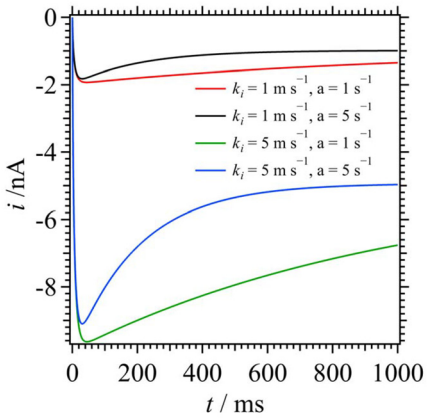

Fig. 7 Simulated chronoamperograms generated using the finite element simulation described in ESI section 7† for the k_i and a values indicated in the inset.

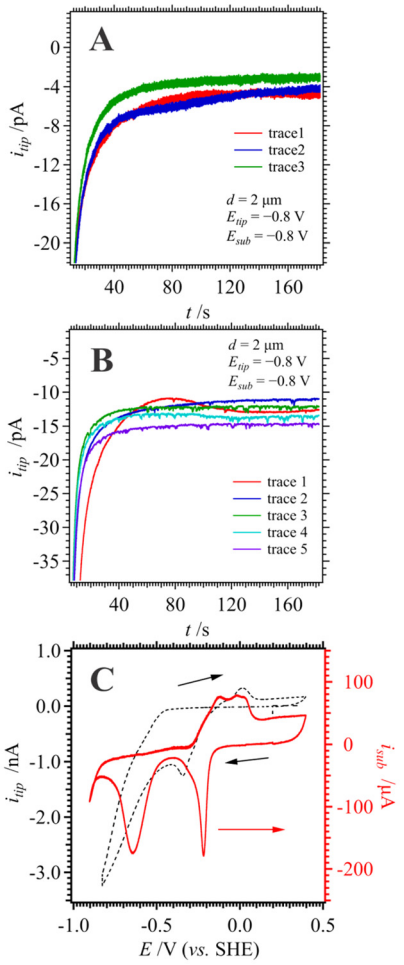

Fig. 8 (A) Chronoamperograms recorded at i_{tip} while E_{sub} and E_{tip} were maintained at a cathodic potentials in a $KHCO_3$ (pH 10) solution, and then (B) after performing the CVs depicted (C) at 0.020 V s^{-1}. Red arrow indicates the current axis plotted against.

in which we define k_i as the initial standard rate constant, a as the decay coefficient, and t as time. Eqn (9) is an approximation; however, it provides a straightforward, semi-empirical means of understanding k° and passivation as a function of time with the addition of only 2 other coefficients. k_i describes the initial spike intensity (in units of m s^{-1}), while a defines the curvature of the exponential decay current profile (expressed in units of s^{-1}). Employing eqn (9), k_i values 2× that expected of k° values for a steady state condition were necessary to achieve the i–t spike profiles shown in Fig. 7. For the experimentally observed current range of i_p = 6–20 pA, k_i = 0.0033–0.011 m s^{-1} was required with the CuO NP positioned flat on the UME surface, as depicted in Fig. S15 of the ESI;† these k_i values translate into k° = 0.0066–0.022 m s^{-1} at t = 0 s, and 0.0045–0.015 m s^{-1} at t = 0.2 s. Meanwhile, an a = 5 s^{-1} was used throughout.

As mentioned above,[12,14] if anodic potentials are avoided, then Cu polycrystalline morphological changes can be avoided, and likely Cu NP ejection is inhibited. Fig. 8A depicts the i–t responses if E_{sub} is first maintained at a high cathodic potential which results in no detectable NP collisions. However, after performing CVs at the UME and substrate (Fig. 8C) and then pulsing both negatively, small NP impacts were observed with i_p = 267 ± 4 fA (Fig. 8B). These would be indicative of much smaller Cu oxide NPs being ejected likely owing to the much less aggressive oxidation of the Cu substrate *versus* the experiments shown in Fig. 3 and 6. These data agree with the dissolution mechanism proposed by Speck and Cherevko[12] as well as Koper's group,[14] wherein only through accidental surface oxidation does Cu suffer morphological restructuring or loss.

4. Conclusions

In summary, anodic ejection of Cu^0/Cu oxide NPs was evidenced through TEM imaging of aqueous samples as well as SEE *via* a UME positioned close to a Cu(poly) substrate. Finite element simulations permit the estimation of initial catalytic rate constants when compared to i_p values observed through NP stochastic impacts. However, these simulations rely on several assumptions, chiefly that the ESA of the UME does not change which, as demonstrated herein, is false. Indeed, as shown through SEM imaging of the UME tip post electrolysis, there is simultaneous Cu electrodeposition and electrocatalytic CO_2R at the UME interface resulting in the growth of a flower-like Cu deposit on the carbon fibre UME. Interestingly, if the Cu substrate is maintained at cathodic potentials, then no NP ejection was observed; however, once a modest anodic pulse is applied, then even with E_{sub} = −0.8 V NP collisions were recorded. However, the i_p intensity associated with those impacts was greatly reduced relative to applying E_{sub} = 0.3 V. This means, however, that SECM-SG/TC is a promising electroanalytical tool for quantification of metal corrosion through SEE. One remaining bottleneck is to deconvolute the SEE signal brought about by Cu electrodeposition on its surface likely accompanied by morphological changes.

Thus, future work will include creating a finite element or MD simulation which accounts for growth of a Cu^0/Cu oxide deposit on the UME surface and its influence on the NP stochastic impact frequency. Interestingly, the ECA of the OER does not suffer as much from Cu/Cu oxide NP accumulation; however, it is still present and something that needs to be accounted for during Cu NP corrosion monitoring.

To the best of our knowledge, SEE has never been applied to corrosion studies in this manner before. Thus, this provides a completely new approach to the field and will aid in the fundamental understanding of Cu-mediated CO_2R catalysis.

Author contributions

O.N.E.: formal analysis, investigation, writing – review & editing, data curation, and validation. B.H.P.M.: formal analysis, software, writing – review & editing, and validation. F.M.K.: conceptualization, methodology, supervision, writing – review & editing, project administration, and funding acquisition. T.J.S.: conceptualization, methodology, supervision, writing – original draft, writing – review & editing, project administration, and funding acquisition.

Data availability

All data from this research will be made available on the Borealis Dataverse database repository **https://borealisdata.ca/dataverse/memorial**.

Conflicts of interest

There are no conflicts to declare.

Acknowledgements

T. J. S. is grateful to the Natural Sciences and Engineering Research Council (NSERC) for a Discovery Grant (#006074-2019) as well as the Canadian Foundation for Innovation (CFI) and Memorial University (MUN) for infrastructure funding. O. N. E. is thankful for the Dr Liqin Chen Scholarship fund and MUN CREAIT network for access to instrumentation. F. M. K. and O. N. E. thank the NSERC CREATE program 'Circuit' (**https://www.circuitco2.ca/**) for scholarship funding.

References

1 J. Yang, J. Jiao, S. Liu, Y. Yin, Y. Cheng, Y. Wang, M. Zhou, W. Zhao, X. Tong, L. Jing, P. Zhang, X. Sun, Q. Zhu, X. Kang and B. Han, *Angew. Chem., Int. Ed.*, 2024, **63**, e202410145.
2 X. Hu, Z. Zhang, Z. Li, Y. Wu, W. Wei, Y. Wang, J. Xu and M. Ding, *Appl. Catal., B*, 2024, **358**, 124445.
3 W. Tang, A. A. Peterson, A. S. Varela, Z. P. Jovanov, L. Bech, W. J. Durand, S. Dahl, J. K. Nørskov and I. Chorkendorff, *Phys. Chem. Chem. Phys.*, 2012, **14**, 76–81.
4 D. A. Lowy, J. R. Melendez and B. Mátyás, *Renewable Sustainable Energy Rev.*, 2024, **194**, 114300.
5 Z. Zhang, H. Li, Y. Shao, L. Gan, F. Kang, W. Duan, H. A. Hansen and J. Li, *Nat. Commun.*, 2024, **15**, 612.
6 C.-T. Dinh, T. Burdyny, M. G. Kibria, A. Seifitokaldani, C. M. Gabardo, F. P. García de Arquer, A. Kiani, J. P. Edwards, P. De Luna, O. S. Bushuyev, C. Zou, R. Quintero-Bermudez, Y. Pang, D. Sinton and E. H. Sargent, *Science*, 2018, **360**, 783–787.
7 C. Long, X. Liu, K. Wan, Y. Jiang, P. An, C. Yang, G. Wu, W. Wang, J. Guo, L. Li, K. Pang, Q. Li, C. Cui, S. Liu, T. Tan and Z. Tang, *Sci. Adv.*, 2023, **9**, eadi6119.
8 P. Grosse, A. Yoon, C. Rettenmaier, A. Herzog, S. W. Chee and B. Roldan Cuenya, *Nat. Commun.*, 2021, **12**, 6736.
9 Y.-G. Kim, J. H. Baricuatro, A. Javier, J. M. Gregoire and M. P. Soriaga, *Langmuir*, 2014, **30**, 15053–15056.
10 J. Vavra, G. P. L. Ramona, F. Dattila, A. Kormányos, T. Priamushko, P. P. Albertini, A. Loiudice, S. Cherevko, N. Lopéz and R. Buonsanti, *Nat. Catal.*, 2024, **7**, 89–97.
11 S. Popovic, M. Bele and N. Hodnik, *ChemElectroChem*, 2021, **8**, 2634–2639.
12 F. D. Speck and S. Cherevko, *Electrochem. Commun.*, 2020, **115**, 106739.
13 D. Zhong, D. Cheng, Q. Fang, Y. Liu, J. Li and Q. Zhao, *Chem. Eng. J.*, 2023, **470**, 143907.
14 S. J. Raaijman, N. Arulmozhi and M. T. M. Koper, *ACS Appl. Mater. Interfaces*, 2021, **13**, 48730–48744.
15 A. H. Zewail, *Science*, 2010, **328**, 187–193.
16 B. Beverskog and I. Puigdomenech, *J. Electrochem. Soc.*, 1997, **144**, 3476.
17 E. Mena-Morcillo, A. Ebrahimzadeh Pilehrood, R. Moshrefi, G. Shafiee, P. G. Keech, M. Behazin and S. M. Gateman, *Anal. Chem.*, 2024, **96**, 9122–9131.
18 X. Xu, D. Valavanis, P. Ciocci, S. Confederat, F. Marcuccio, J.-F. Lemineur, P. Actis, F. Kanoufi and P. R. Unwin, *Anal. Chem.*, 2023, **95**, 319–356.
19 O. N. Egbe, B. H. P. Morrissey, N. E. Harvey, C. Schneider, L. S. Cahill and T. J. Stockmann, *J. Electroanal. Chem.*, 2023, **945**, 117678.
20 N. Ahmadinasab and T. J. Stockmann, *ChemElectroChem*, 2022, **9**, e202200162.
21 T. J. Stockmann, J.-F. Lemineur, H. Liu, C. Cometto, M. Robert, C. Combellas and F. Kanoufi, *Electrochim. Acta*, 2019, **299**, 222–230.
22 T. J. Stockmann, L. Angelé, V. Brasiliense, C. Combellas and F. Kanoufi, *Angew. Chem., Int. Ed.*, 2017, **56**, 13493–13497.
23 S. V. Sokolov, S. Eloul, E. Katelhon, C. Batchelor-McAuley and R. G. Compton, *Phys. Chem. Chem. Phys.*, 2017, **19**, 28–43.
24 B. M. Quinn, P. G. van't Hof and S. G. Lemay, *J. Am. Chem. Soc.*, 2004, **126**, 8360–8361.

25 X. Xiao and A. J. Bard, *J. Am. Chem. Soc.*, 2007, **129**, 9610–9612.
26 H. Le, C. Lin, E. Kätelhön and R. G. Compton, *Electrochim. Acta*, 2019, **298**, 778–787.
27 P. Ciocci, D. Valavanis, G. N. Meloni, J. F. Lemineur, P. R. Unwin and F. Kanoufi, *ChemElectroChem*, 2023, e202201162.
28 M. M. Vieira, J.-F. Lemineur, J. Médard, C. Combellas, F. Kanoufi and J.-M. Noël, *J. Phys. Chem. Lett.*, 2022, 5468–5473, DOI: 10.1021/acs.jpclett.2c01408.
29 V. Brasiliense, J. Clausmeyer, A. L. Dauphin, J.-M. Noël, P. Berto, G. Tessier, W. Schuhmann and F. Kanoufi, *Angew. Chem., Int. Ed.*, 2017, **56**, 10598–10601.
30 S.-X. Guo, C. L. Bentley, M. Kang, A. M. Bond, P. R. Unwin and J. Zhang, *Acc. Chem. Res.*, 2022, **55**, 241–251.
31 E. Daviddi, V. Shkirskiy, P. M. Kirkman, M. P. Robin, C. L. Bentley and P. R. Unwin, *Chem. Sci.*, 2021, **12**, 3055–3069.
32 B. Chen, D. Perry, J. Teahan, I. J. McPherson, J. Edmondson, M. Kang, D. Valavanis, B. G. Frenguelli and P. R. Unwin, *ACS Meas. Sci. Au*, 2021, **1**(1), 6–10.
33 Y. Zhang, M. A. Edwards, S. R. German and H. S. White, *J. Phys. Chem. C*, 2016, **120**, 20781–20788.
34 S. R. German, T. S. Hurd, H. S. White and T. L. Mega, *ACS Nano*, 2015, **9**, 7186–7194.
35 M. Azimzadeh Sani and K. Tschulik, *Curr. Opin. Electrochem.*, 2023, **37**, 101195.
36 M. Jaugstetter, N. Blanc, M. Kratz and K. Tschulik, *Chem. Soc. Rev.*, 2022, **51**, 2491–2543.
37 V. Brasiliense, J.-M. Noël, K. Wonner, K. Tschulik, C. Combellas and F. Kanoufi, *ChemElectroChem*, 2018, **5**, 3036–3043.
38 S.-M. Lu, M. Chen, H. Wen, C.-B. Zhong, H.-W. Wang, Z. Yu and Y.-T. Long, *J. Am. Chem. Soc.*, 2024, **146**(22), 15053–15060.
39 J. Zhang, W. He, T. Quast, J. R. C. Junqueira, S. Saddeler, S. Schulz and W. Schuhmann, *Angew. Chem., Int. Ed.*, 2023, **62**, e202214830.
40 T. H. T. Nguyen, J. Lee, H.-Y. Kim, K. M. Nam and B.-K. Kim, *Biosens. Bioelectron.*, 2020, **151**, 111999.
41 A. K. Shukla, D. Park and B. Kim, *Anal. Chim. Acta*, 2024, **1319**, 342964.
42 W. Yi, J. Xiao, Z. Shi, C. Zhang, L. Yi, Y. Lu and X. Wang, *Analyst*, 2024, **149**, 4981–4996.
43 S. G. Lemay, C. Renault and J. E. Dick, *Curr. Opin. Electrochem.*, 2023, 101265, DOI: 10.1016/j.coelec.2023.101265.
44 A. Langlard, H. Smida, R. Chevalet, C. Thobie-Gautier, M. Boujtita and E. Lebègue, *ACS Meas. Sci. Au*, 2024, **4**, 585–592.
45 L. K. Allerston and N. V. Rees, *Curr. Opin. Electrochem.*, 2018, **10**, 31–36.
46 P. H. Robbs and N. V. Rees, *Phys. Chem. Chem. Phys.*, 2016, **18**, 24812–24819.
47 N. V. Rees, *Electrochem. Commun.*, 2014, **43**, 83–86.
48 S.-M. Lu, J.-F. Chen, Y.-Y. Peng, W. Ma, H. Ma, H.-F. Wang, P. Hu and Y.-T. Long, *J. Am. Chem. Soc.*, 2021, **143**, 12428–12432.
49 V. J. Keast, *Appl. Nanosci.*, 2022, **12**, 1859–1868.
50 Q. Liu, Q. Jiang, L. Li and W. Yang, *J. Am. Chem. Soc.*, 2024, **146**, 4242–4251.
51 N. Bodappa, M. Su, Y. Zhao, J.-B. Le, W.-M. Yang, P. Radjenovic, J.-C. Dong, J. Cheng, Z.-Q. Tian and J.-F. Li, *J. Am. Chem. Soc.*, 2019, **141**, 12192–12196.
52 S. Mu, H. Lu, Q. Wu, L. Li, R. Zhao, C. Long and C. Cui, *Nat. Commun.*, 2022, **13**, 3694.
53 P. Vanýsek, in *CRC Handbook of Chemistry and Physics*, ed. W. M. Haynes, CRC Press/Taylor, Boca Raton, FL, 2021, pp. 8.20–28.29.
54 J. Heinze, A. Rasche, M. Pagels and B. Geschke, *J. Phys. Chem. B*, 2007, **111**, 989–997.
55 R. Moshrefi, E. P. Connors, E. Merschrod and T. J. Stockmann, *Electrochim. Acta*, 2022, **426**, 140749.
56 L. Nazari and T. J. Stockmann, *Langmuir*, 2024, **40**, 24494–24506.
57 R. A. Lehane, A. Gamero-Quijano, J. A. Manzanares and M. D. Scanlon, *J. Am. Chem. Soc.*, 2024, **146**, 28941–28951.
58 X. Liu, P. Schlexer, J. Xiao, Y. Ji, L. Wang, R. B. Sandberg, M. Tang, K. S. Brown, H. Peng, S. Ringe, C. Hahn, T. F. Jaramillo, J. K. Nørskov and K. Chan, *Nat. Commun.*, 2019, **10**, 32.
59 E. Laborda, A. Molina, V. F. Espín, F. Martínez-Ortiz, J. García de la Torre and R. G. Compton, *Angew. Chem., Int. Ed.*, 2017, **56**, 782–785.
60 C. D. Cwalina, K. J. Harrison and N. J. Wagner, *Soft Matter*, 2016, **12**, 4654–4665.
61 D. J. Audus, A. M. Hassan, E. J. Garboczi and J. F. Douglas, *Soft Matter*, 2015, **11**, 3360–3366.
62 L. C. R. Alfred and K. B. Oldham, *J. Phys. Chem.*, 1996, **100**, 2170–2177.
63 Y. Deng, A. D. Handoko, Y. Du, S. Xi and B. S. Yeo, *ACS Catal.*, 2016, **6**, 2473–2481.
64 J. Feng, Y. Wang, X. Lin, M. Bian and Y. Wei, *Surf. Coat. Technol.*, 2023, **459**, 129411.
65 F. Li, C. Zhou and A. Klinkova, *Phys. Chem. Chem. Phys.*, 2022, **24**, 25695–25719.
66 F. Li, X. V. Medvedeva, J. J. Medvedev, E. Khairullina, H. Engelhardt, S. Chandrasekar, Y. Guo, J. Jin, A. Lee, H. Thérien-Aubin, A. Ahmed, Y. Pang and A. Klinkova, *Nat. Catal.*, 2021, **4**, 479–487.